# Alterations in the Choriocapillaris in Intermediate Age-Related Macular Degeneration

Enrico Borrelli,[1–3] Akihito Uji,[1,2] David Sarraf,[4,5] and SriniVas R. Sadda[1,2]

[1]Doheny Image Reading Center, Doheny Eye Institute, Los Angeles, California, United States
[2]Department of Ophthalmology, David Geffen School of Medicine at UCLA, Los Angeles, California, United States
[3]Ophthalmology Clinic, Department of Medicine and Science of Ageing, University G. D'Annunzio Chieti-Pescara, Chieti, Italy
[4]Retinal Disorders and Ophthalmic Genetics Division, Stein Eye Institute, David Geffen School of Medicine at UCLA, Los Angeles, California, United States
[5]Greater Los Angeles VA Healthcare Center, Los Angeles, California, United States

**PURPOSE.** The purpose of this study was to compare the choriocapillaris plexus in eyes with intermediate AMD (iAMD), with or without neovascular AMD in the fellow eye, using optical coherence tomography angiography (OCTA).

**METHODS.** We collected data from 42 eyes with iAMD from 42 patients who had obtained OCTA. This cohort was divided into two subgroups according to the status of the fellow eye, yielding a group of 20 cases with bilateral intermediate AMD (bilateral iAMD group) and 22 cases with neovascular AMD in the fellow eye (unilateral iAMD group). An additional control group of 20 eyes from 20 healthy subjects was included for comparison. Main outcome measures were: (1) the percent of nondetectable perfused choriocapillaris area and (2) the average choriocapillaris signal void size.

**RESULTS.** No differences in the percent of nondetectable perfused choriocapillaris area were found among the three groups (2.3 ± 1.4% in the unilateral iAMD group, 1.5 ± 0.9% in the bilateral iAMD group, and 1.7 ± 1.4% in the control group, respectively). The average choriocapillaris signal void size, however, was significantly increased in unilateral iAMD eyes (293.7 ± 71.2 μm$^2$) compared to both bilateral iAMD (241.5 ± 51.6 μm$^2$, $P = 0.031$) and control (212.7 ± 48.6 μm$^2$, $P = 0.001$) eyes.

**CONCLUSIONS.** Intermediate AMD eyes of patients with neovascular AMD in the fellow eye have an increased average choriocapillaris signal void size compared to eyes without neovascular AMD in the fellow eye. If replicated in future studies, choriocapillaris signal void size may prove to be a useful parameter for evaluating eyes with AMD.

Keywords: age-related macular degeneration, image analysis, choriocapillaris, retina

AMD is the leading cause of irreversible central vision loss among older individuals in developed countries.[1] Intermediate AMD (iAMD) is clinically characterized by the accumulation of drusen and can progress to the late form of AMD notable for choroidal (type 1 and 2) or retinal neovascularization (type 3) or geographic atrophy (GA).

AMD is a complex disease with multifactorial etiologies. Although many factors have been implicated in the pathogenesis and progression of this disorder,[2,3] including inflammation, oxidative damage, aging, genetic predisposition, and environmental influences, there is strong evidence that AMD ultimately may be characterized by damage of the retinal pigment epithelium (RPE), Bruch's membrane, and choriocapillaris (CC) complex.[4,5] The dysfunction of this unit leads to the development of drusen between the RPE and Bruch's membrane complex and progressive RPE and CC loss and photoreceptor atrophy.

Histopathologic abnormalities of the CC have been studied extensively in AMD eyes. The CC is a uniform meshwork of densely packed and interconnected capillaries, and the number of nonperfused capillary segments (called ghost vessels) has been shown to be increased in the presence of drusen.[6–8]

Furthermore, the choroid of iAMD eyes with neovascular AMD (nAMD) in the fellow eye was significantly thinner than that in healthy eyes, while the choroidal thickness of those patients with bilateral iAMD did not differ from control eyes.[9] Given that the fellow eyes of patients with unilateral nAMD are known to be at a higher risk of late AMD,[10,11] choroidopathy may play an important role in the development of choroidal neovascularization (CNV) or GA.

Optical coherence tomography angiography (OCTA) has evolved into a useful imaging technology and has provided the capability to evaluate the retinal and anterior choroidal vascular circulations without the need for dye injection. In the OCTA CC scans, dark regions referred to as flow voids may alternate with granular bright areas, and this pattern may systematically change with age or myopia.[12,13] The latter may represent CC flow, while the former more may be secondary to CC dropout.[14] It is important to note that the detectable flow range of OCTA is limited, and flows below the decorrelation threshold are indistinguishable from background noise and are thus undetectable.[15] Considering this, CC flow voids have recently been renamed signal voids.[16] With advanced image-processing software, quantification of the total number and the

4792

total and average area of these CC signal voids is now possible.[12]

The main aim of this study was to explore quantitative differences in the CC of patients affected by iAMD, with or without nAMD in the fellow eye, using OCTA analysis.

## METHODS

### Study Participants

In this retrospective cohort study, subjects 50 years of age and older with iAMD[17] in one eye and iAMD or nAMD in the fellow eye were identified from the medical records of a medical retinal practice (DS) at the UCLA Stein Eye institute. The study was approved by the UCLA Institutional Review Board (IRB) and adhered to the tenets of the Declaration of Helsinki and Health Insurance Portability and Accountability Act.

All patients were imaged with OCTA (RTVue XR Avanti AngioVue; Optovue, Inc., Fremont, CA, USA) between July 2014 and October 2016. An IRB-approved informed consent was obtained from all patients. Moreover, all patients received a complete ophthalmologic examination, which included the measurement of best-corrected visual acuity (BCVA), IOP, and dilated fundus examination.

The inclusion criteria for iAMD eyes included having drusen >125 μm in diameter with or without pigmentary abnormalities as assessed by clinical examination and confirmed by dense volume OCT (pigment abnormalities on OCT manifesting as intraretinal hyperreflective features). Exclusion criteria for iAMD eyes were (1) presence of pseudodrusen on the OCT scan; (2) previous ocular surgery or history of antivascular VEGF therapy; (3) any maculopathy secondary to causes other than AMD (including presence of an epiretinal membrane or vitreomacular traction syndrome); (4) myopia greater than −3.00 diopters; and (5) any optic neuropathy, including glaucoma. Furthermore, we excluded poor-quality images with a strength index less than 40, with either significant motion artifact (seen as large dark lines on the en face angiogram) or incorrect segmentation at the level of the superficial capillary plexus (SCP) and CC.

Assuming age may affect retinal and choroidal features measured by means of OCTA,[12,18] a control group matched for age and sex was also included in the current analysis. All control subjects were volunteers with no evidence of retinal disease or ocular media opacity as evaluated by dilated fundus examination and OCTA.

### Imaging

Patients underwent OCTA imaging using the RTVue XR Avanti spectral-domain OCT device with a light source at 840 nm, a bandwidth of 45 nm, and an A-scan rate of 70,000 scans per second. This device is equipped with the AngioVue software (version 2016.1.0.26; Optovue, Inc.), which is based on a split-spectrum amplitude-decorrelation angiography (SSADA) algorithm.[19] A 3 × 3-mm cube centered in the fovea containing 304 × 304 A-scans was acquired. Each B-scan was repeated at each cross-section in the fast-scan axis to separate static tissue from blood-flow signals. Two OCTA volume scans with orthogonal fast-scan directions (horizontal and vertical) were acquired for each eye and then merged by the software to minimize motion artifact.[20,21]

### Image Processing

The main outcome measures were (1) the percent non-detectable perfused CC area (PNPCA), which represents a measure of the total area of CC vascular dropout, and (2) the average CC signal void size.

In order to evaluate the PNPCA (Fig. 1), we tested the percentage of pixels in the CC en face image (slab 30-μm thick starting 31 μm posterior to the RPE reference) below a nonperfusion (noise-level) threshold. Previous studies have investigated this threshold either in the foveal avascular zone[22] or in the avascular outer retina.[23] In brief, for each patient we first exported the 32-bit en face OCTA scan of the avascular outer retina (slab with an inner boundary located 70 μm below the inner plexiform layer and an outer boundary located 30 μm below the RPE reference). The avascular outer retina image was then imported into image analysis ImageJ software version 1.50 (http://rsb.info.nih.gov/ij/index.html; provided in the public domain by National Institutes of Health, Bethesda, MD),[24] and the nonperfusion threshold was calculated as the mean of all the pixel values. This threshold was applied to the 32-bit en face CC OCTA scan imported into ImageJ.

The CC directly beneath drusen, as well as under superficial retinal vessels, was excluded from the analysis to avoid shadowing or projection artifacts confounding the analysis.[25] To identify the drusen area, we used the RPE elevation map elaborated by the AngioVue software. This image was imported into ImageJ, and the Split Channels function was carried on to obtain the green channel image. In the latter image, the RPE elevation area appears darker then the surrounding area, as confirmed by two Doheny Eye Institute–certified graders (EB and AU). The MaxEntropy threshold was therefore applied to "binarize" the obtained image. The SCP en face OCTA image was segmented with an inner boundary 3 μm below the internal limiting membrane and an outer boundary set at 15 μm below the inner plexiform layer. Also, the 32-bit SCP image was opened in ImageJ, and the MaxEntropy threshold was applied to visualize only the greater superficial retinal vessels (causing shadowing and artifacts). The same two graders confirmed these observations (Fig. 1).

The three obtained thresholded images were then merged by means of image analysis GNU Image Manipulation Program (GIMP) software (version 2.8.16; available at https://www.gimp.org) in order to allow analysis of the CC layer after identification and removal of the drusen and superficial vessel regions. The resultant image (Fig. 2) was then analyzed in Image J, and the following evaluations were performed: (1) the Analyze Particles command, which measured and counted all thresholded areas greater or equal to one pixel where there was a lack of flow information, furnished us the number, average, and maximum size of the signal voids and (2) the PNPCA, calculated as the number of pixels falling below the threshold (the total area of the signal voids) divided by the total number of pixels in the remaining analyzed area of CC, as follows:

$$PNPCA = \frac{\sum SVS1 + SVS2 + \ldots + SVSn}{Total\ CC\ area - (Drusen\ area + SCP\ area)} \times 100$$

$$(1)$$

where SVS is the size of each signal void. The average CC signal void size was calculated as the sum of all the signal voids' sizes divided by the total number of detected signal voids.

Finally, we evaluated the PNPCA in the 150-μm-wide ring around the drusen edge (Fig. 3). We used this peri-drusen ring because analysis of the CC directly beneath the drusen may be confounded by signal loss through the drusen.[25] To obtain this ring, we used the Distance Map ImageJ function on the RPE elevation image already elaborated and binarized. This function provided delineation of a border 150 μm displaced from the drusen edge. Furthermore, the Distance Map function on the binarized image allowed delimiting those areas within 150 μm
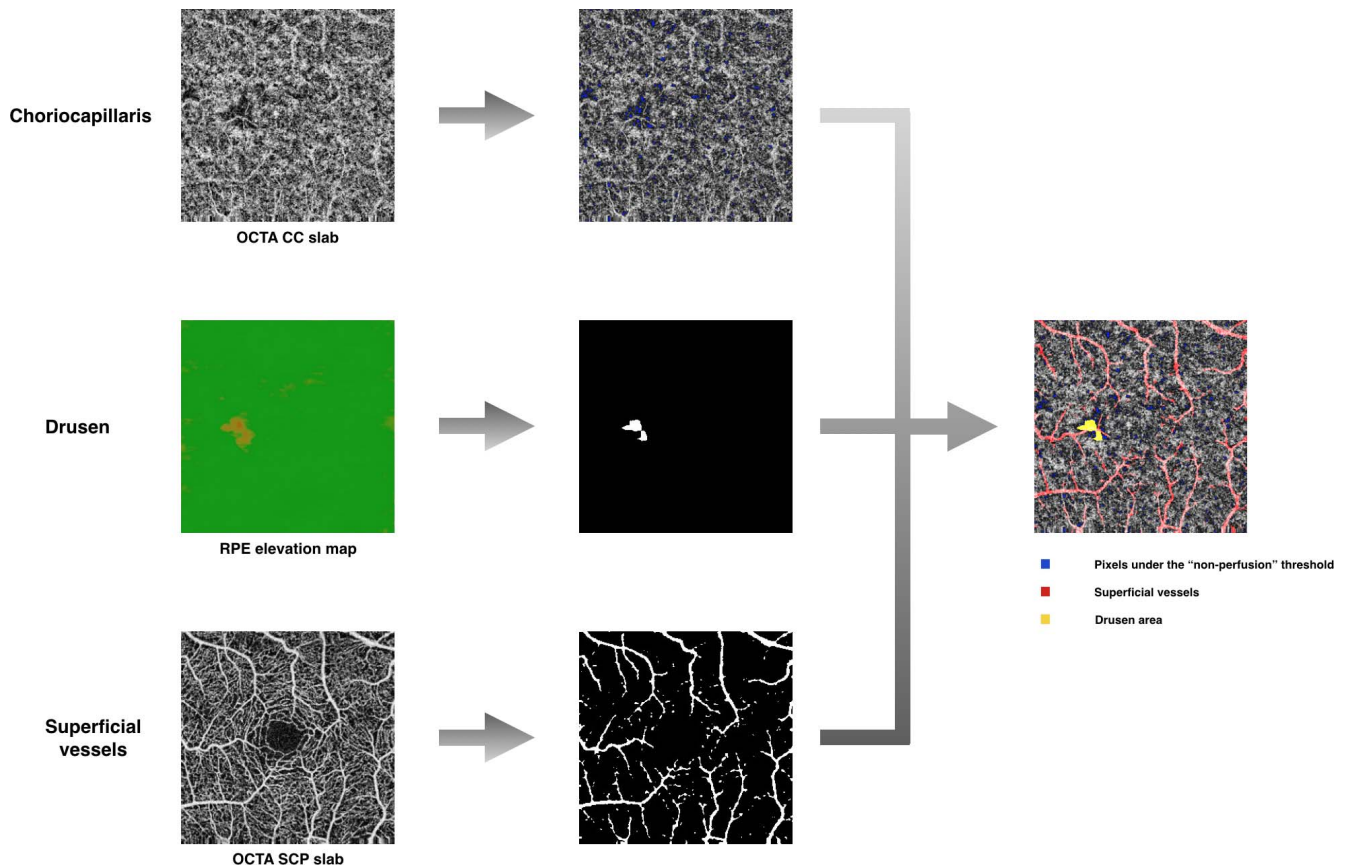
**FIGURE 1.** Representation of the algorithm used to investigate the nondetectable perfused CC. To evaluate the percent nondetectable PNPCA, we tested the percentage of pixels (*blue dots*) in the CC en face image below a nonperfusion threshold, which was calculated as the mean of all the pixel values in the outer avascular retina. To identify and mask both the drusen (*yellow*) and the SCP vessel (*red*) areas, we used the RPE elevation map and the SCP en face OCTA images, which were thresholded and binarized. The three obtained thresholded images were then merged. Finally, the PNPCA was obtained by dividing the area below the threshold by the remaining area of CC.

from the edge of all the drusen in the image (without any size limit) by excluding areas occupied by adjacent drusen.

## Statistical Analysis

Statistical calculations were performed using Statistical Package for Social Sciences (version 20.0; SPSS, Inc., Chicago, IL, USA). To detect departures from normality distribution, the Shapiro-Wilk's test was performed for all variables. All quantitative variables were presented as media and standard deviation in the results and table. Continuous variables were compared by conducting a 1-way analysis of covariance (ANCOVA) with Bonferroni post hoc test, by introducing age as covariate. Student's *t*-test was used to compare the drusen area between the two iAMD groups. Pearson's correlation was performed to evaluate the linear correlation among variables in patients with AMD.
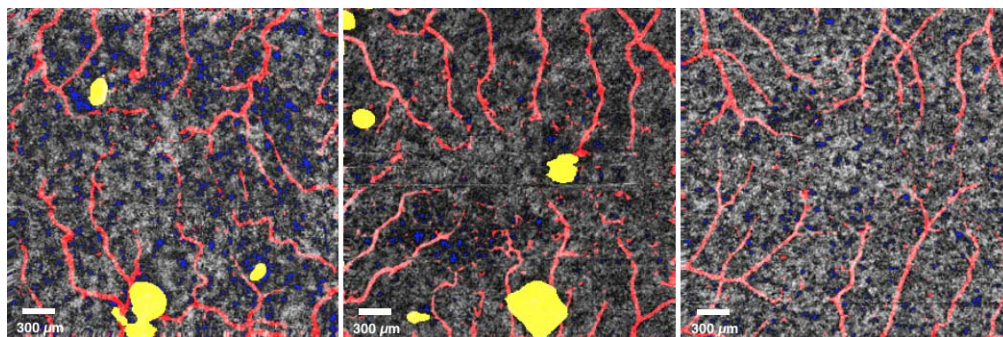


**FIGURE 2.** Representative post-processed OCTA CC images. Representative OCTA 3 × 3-mm scans segmented at the CC plexus from a unilateral iAMD patient (*left*), a bilateral iAMD patient (*middle*), and a healthy control (*right*). The CC beneath drusen (*yellow area*) and superficial vessels (*red area*) was not investigated. The percent nondetectable PNPCA was obtained by dividing the area below the nonperfusion threshold (*blue dots*) by the remaining area of CC.
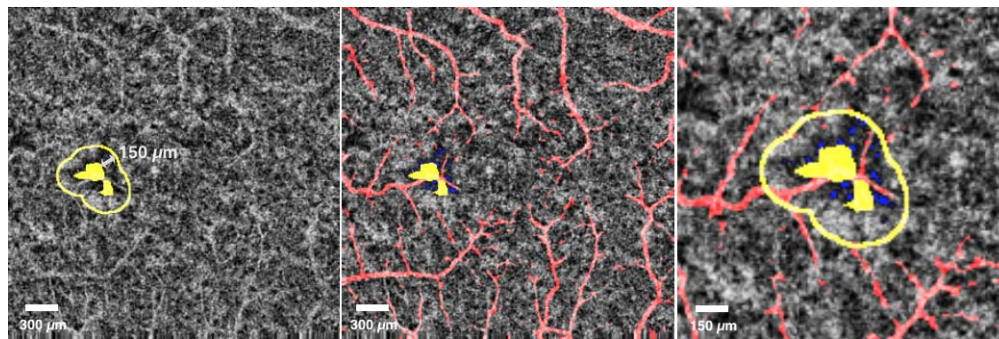
Investigative Ophthalmology & Visual Science

**FIGURE 3.** Representative post-processed OCTA CC images highlighting the ring around the drusen edge. The percent nondetectable PNPCA was also tested in the 150-μm-wide ring around the drusen edge. After excluding the CC beneath drusen (*yellow area*) and superficial vessels (*red area*), we automatically delineated a border 150 μm from the drusen area edge (*left image*). We tested the percentage of pixels (*blue dots*) below the nonperfusion threshold in this ring (*middle image*). A higher magnification of the tested area is visible in the right image.

In the PNPCA analysis in the 150-μm-wide ring around the drusen edge, though healthy controls do not have drusen area, we considered the whole PNPCA for these subjects in the comparison with the AMD groups.

The BCVA for each eye was converted to the logarithm of the minimum angle of resolution (LogMAR), as previously described.[26]

The chosen level of statistical significance was $P < 0.05$.

## RESULTS

### Characteristics of Patients Included in the Analysis

Of the 62 patients included in this analysis, 22 (10 female) had iAMD eyes with nAMD in the fellow eye (unilateral iAMD group), 20 (12 female) were affected by bilateral iAMD (bilateral iAMD group), and 20 (10 female) were healthy controls. To avoid bias, in the bilateral iAMD group we included only the left eye in the analysis, except for three patients in whom the right eye was analyzed instead because of scan quality (two patients) or because of the diagnosis of amblyopia (one patient) in the left eye.

Mean $\pm$ SD age was $78.7 \pm 7.9$ years (range, 60–89 years) in the unilateral iAMD group, $73.5 \pm 8.0$ years (range, 60–87 years) in the bilateral iAMD group, and $73.1 \pm 6.4$ years (range, 66–89 years) in the control group ($P > 0.05$ for all the comparisons). Moreover, no difference in BCVA ($0.17 \pm 0.13$ LogMAR in unilateral iAMD patients, $0.17 \pm 0.15$ LogMAR in bilateral iAMD patients, and $0.00 \pm 0.0$ LogMAR in healthy subjects) was found between the two AMD groups.

The drusen area was $1.1 \pm 0.3$ mm$^2$ in unilateral iAMD and $1.0 \pm 0.4$ mm$^2$ in bilateral iAMD ($P = 0.297$).

### Percent Nondetectable Perfused CC Area

The whole PNPCA (Table; Fig. 4) was $2.3 \pm 1.4\%$ in the unilateral iAMD group ($P = 0.714$ in the comparison with healthy subjects, $P = 0.293$ in the comparison with bilateral iAMD patients, respectively); $1.5 \pm 0.9\%$ in the bilateral iAMD group ($P = 1.0$ in the comparison with the control group); and $1.7 \pm 1.4\%$ in the control group.

In the evaluation of the CC layer in the 150-μm-wide ring around the drusen edge, the PNPCA was significantly increased in unilateral iAMD eyes compared to control eyes ($4.7 \pm 4.9\%$, $P = 0.018$), but was *not* increased in the bilateral iAMD eyes ($2.6 \pm 1.9\%$, $P = 1.0$).

### Signal Void Analysis

The average signal void size (Table; Fig. 4) was increased in those patients affected by unilateral iAMD ($293.7 \pm 71.2$ μm$^2$), compared with both control subjects ($212.7 \pm 48.6$ μm$^2$, $P = 0.001$), and bilateral iAMD patients ($241.5 \pm 51.6$ μm$^2$, $P = 0.031$).

Neither the number nor the maximum size of the CC signal void differed among the three groups (Table).

### Correlation Analysis

The whole PNPCA did not correlate with age ($R^2 = 0.246$, $P = 0.117$), BCVA ($R^2 = -0.215$, $P = 0.209$), or drusen area ($R^2 = 0.125$, $P = 0.432$). The average signal void size did not show

**TABLE.** Tested Parameters in iAMD Patients and Controls

| Tested Parameters | Unilateral iAMD Group, $n = 22$ | Bilateral iAMD Group, $n = 20$ | Control Group, $n = 20$ | Unilateral iAMD vs. Controls *P* Value | Bilateral iAMD vs. Controls *P* Value | Unilateral iAMD vs. Bilateral iAMD *P* Value |
|---|---|---|---|---|---|---|
| PNPCA, % | | | | | | |
| Total area | $2.3 \pm 1.4$ | $1.5 \pm 0.9$ | $1.7 \pm 1.4$ | 0.714 | 1.0 | 0.293 |
| Drusen ring area | $4.7 \pm 4.7$ | $2.6 \pm 1.9$ | $1.7 \pm 1.4$ | 0.018 | 1.0 | 0.145 |
| CC signal void | | | | | | |
| Number, $n$ | $589.8 \pm 343.4$ | $507.7 \pm 213.1$ | $629.0 \pm 458.7$ | 1.0 | 0.843 | 1.0 |
| Average size, μm$^2$ | $293.7 \pm 71.2$ | $241.5 \pm 51.6$ | $212.7 \pm 48.6$ | 0.001 | 0.373 | 0.031 |
| Maximum size, μm$^2$ | $4625.8 \pm 4410.7$ | $2502.8 \pm 1518.9$ | $2556.3 \pm 3171.4$ | 0.290 | 1.0 | 0.232 |

Data are presented as mean $\pm$ standard deviation.
Values were compared by 1-way ANCOVA with age as covariate, followed by Bonferroni post hoc test.
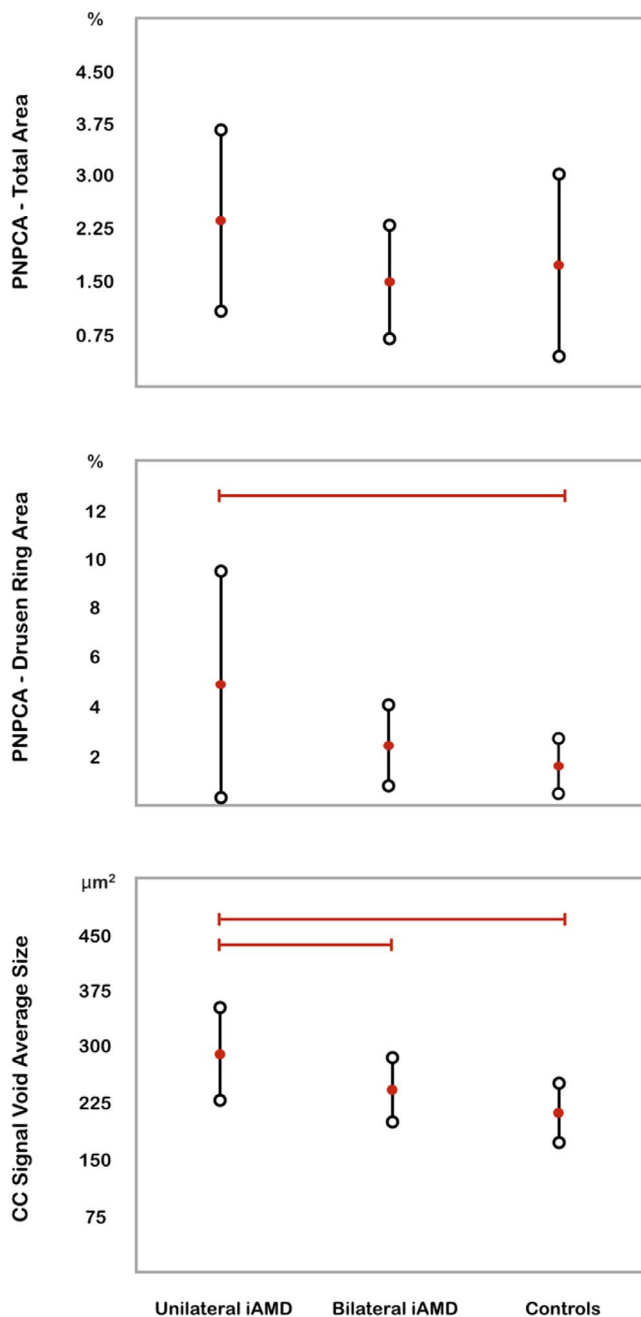
**Figure 4.** Error-bar plot showing analyzed OCTA measurements in AMD patients and healthy controls. Each bar shows mean (*red dot*) and standard deviation (*open circles*) values for each variable. Horizontal *red lines* indicate statistically significant differences between groups (*P* < 0.05).

any significant correlation with age ($R^2 = 0.119$, $P = 0.454$), BCVA ($R^2 = -0.290$, $P = 0.087$) or drusen area ($R^2 = -0.003$, $P = 0.995$).

## Discussion

In this cross-sectional study, we investigated CC features in iAMD eyes. Overall, we found an increased average CC signal void size in iAMD eyes with neovascular AMD in the fellow eye.

Several approaches have been used to demonstrate that microvascular choroidal changes are associated with AMD.

Histopathologic studies have demonstrated that CC alterations are increased with age and the presence of drusen.[6–8] Moreover, the CC dropout has been shown to present at various AMD stages.[27] Since the CC relies on VEGF secretion by the RPE, the presence of drusen could impair this trophic-signaling process and lead to endothelial cell loss.[28] Alternatively, a primary CC vascular loss, due to complement-mediated damage or other genetic and nongenetic factors, may lead to outer retinal layer dysfunction, with impaired removal of debris from Bruch's membrane and RPE ischemia.[29–31] McLeod et al.[32] have extensively studied the causative relationship between outer retinal layer disruption and CC impairment. They analyzed the postmortem choroids from 11 subjects, including three age-matched controls, five GA subjects, and three nAMD subjects. In this study, the choroidal tissues were subsequently embedded in methacrylate and were sectioned in order to evaluate the structural changes. They observed that the CC could remain intact in some areas of GA despite apparent overlying RPE loss. Based on these findings, the authors concluded that the primary insult in GA appears to be at the level of the RPE, with presumed subsequent CC degeneration. In contrast, in nAMD eyes, they observed extensive CC loss (albeit in areas of CNV), despite an apparently intact RPE (at least structurally). The RPE in regions of vascular dropout is likely hypoxic, which may result in an increased VEGF production by the RPE and a consequent stimulation of the CNV growth.

In recent years, OCTA technology has been shown to be useful in studying both iAMD and nAMD eyes. The CC layer has been studied in nAMD eyes to better characterize CNV morphology.[33–35] The retinal and choroidal vasculature in eyes with iAMD has been investigated, and recent studies demonstrated a reduced SCP and CC vessel density in iAMD eyes with nascent GA.[36,37] Spaide[12] has recently investigated the CC flow characteristics by means of OCTA. In this paper, the author showed that the relationship between the number and size of the signal voids followed the following formula (power law): log (number of signal voids) equals a scaling factor times the log (size of signal voids) plus a constant. Interestingly, this constant was shown to be influenced by age, hypertension, and a diagnosis of late AMD in the fellow eye. Furthermore, the total amount of CC vascular dropout recently has been demonstrated to be increased in presence of pseudodrusen.[23]

In our study, the CC average signal void size in unilateral iAMD eyes was demonstrated to be significantly greater compared with healthy eyes, while CC signal void size of bilateral iAMD eyes was not different versus healthy eyes. Moreover, we investigated the PNPCA in our cohort study. We evaluated the PNPCA instead of the total signal void area to account for the differences in area for the region of interest for each subject. The areas of the region of interest varied among subjects because it depended on how much area was excluded due to overlying drusen or superficial vessels. We showed that the PNPCA, while reduced in the presence of pseudodrusen in previous publications,[23] was not statistically significantly different among the three groups in our study (which of course excluded pseudodrusen). This apparent discrepancy between PNPCA and signal void size suggests that there is an increase in the CC density in areas outside of the signal voids. The mechanism for this is uncertain (e.g., could this be a compensatory flow alteration[27]), but further evaluation of this may provide new insights into the pathogenesis of flow alterations over time. The latter finding of adjacent compensatory CC hypervascularity could be related to the RPE becoming hypoxic and producing VEGF, with consequent CC endothelial cell proliferation. Further studies could help shed light on the relationship on this point.

We also evaluated the CC in the 150-µm-wide ring around the drusen edge. The area around the drusen has also been studied by other investigators. Rogala et al.[38] studied the retinal thickness both over drusen and at 150 µm from the drusen border and demonstrated that the retinal thickness is reduced in both these fields. The rationale evaluating the CC in the 150-µm-wide ring around the drusen edge is based on the concept that there is a strict topographic association between drusen appearance and CC dropout.[39,40] Ideally, we would have studied the PNPCA directly below the drusen, but as previously noted, we were concerned about possible signal attenuation with SD-OCTA and hence we used the region immediately adjacent to the drusen as a surrogate. We observed that the PNPCA is reduced in this peri-drusen ring area, but only in the unilateral iAMD group. This additional characteristic also suggests there is increased CC alteration in these eyes.

Taking into consideration that the fellow iAMD eyes of patients with unilateral nAMD are known to be at a higher risk for development of late AMD, our results would seem to corroborate the presence of an ischemic choroidopathy that may predispose to the development of neovascularization and play an important role in the pathophysiology of late AMD. Alternatively, even though the effects on the fellow eye of intravitreal injections of anti-VEGF are still controversial,[41–43] we are not able to exclude that these may explain, at least in part, the CC changes found in unilateral intermediate AMD eyes.

The main limitation of our study is the employment of a single time point for each patient. A prospective longitudinal evaluation of CC vessel density in intermediate AMD patients will shed further light on the role of the CC in late AMD development. Another limitation is inability to evaluate the CC beneath drusen. Nevertheless, it should be considered that CC OCTA images must be interpreted with caution owing to a variety of image artifacts in the presence of drusen.[25] Thus, we felt the safer strategy was to look just at the drusen edge. However, the CC below the drusen and at the margin of drusen may differ. Future studies using swept-source OCTA, which uses a longer wavelength allowing for better RPE penetration and less signal-intensity roll off, should be considered to evaluate this possibility. Furthermore, another limitation is intrinsic to the OCTA device, which is not able to distinguish the absence of flow from that under the slowest detectable flow. A final limitation is that we did not specifically investigate the repeatability of our measurements. However, the repeatability for the PNPCA algorithm was reported previously and was shown to be excellent.[23]

In conclusion, this study investigated the difference in CC flow deficit between healthy control subjects versus eyes with intermediate AMD in both eyes and intermediate AMD with nAMD in the fellow eye. In our study, patients with unilateral iAMD have an increased average CC signal void size compared to control healthy eyes. If replicated in future studies, CC signal void size may prove to be a useful parameter for evaluating eyes with AMD. CC measures may become a novel tool for monitoring the efficacy of novel therapeutic approaches to prevent the development of late AMD.

### Acknowledgments

Disclosure: **E. Borrelli**, None; **A. Uji**, None; **D. Sarraf**, Allergan (F), Genentech (C, F), Regeneron (F), Optovue (C, F); **S.R. Sadda**, Allergan (C, F), Carl Zeiss Meditec (F), Genentech (C, F), Iconic (C), Novartis (C), Optos (C, F), Optovue (C, F), Regeneron (F), Thrombogenics (C)

### References

1. Friedman DS, O'Colmain BJ, Muñoz B, et al. Prevalence of age-related macular degeneration in the United States. *Arch Ophthalmol*. 2004;122:564–572.

2. Klein R, Myers CE, Cruickshanks KJ, et al. Markers of inflammation, oxidative stress, and endothelial dysfunction and the 20-year cumulative incidence of early age-related macular degeneration. *JAMA Ophthalmol*. 2014;132:446.

3. Saksens NTM, Geerlings MJ, Bakker B, et al. Rare genetic variants associated with development of age-related macular degeneration. *JAMA Ophthalmol*. 2016;134:287.

4. Zarbin MA, Rosenfeld PJ. Pathway-based therapies for age-related macular degeneration: an integrated survey of emerging treatment alternatives. *Retina*. 2010;30:1350–1367.

5. Querques G, Rosenfeld PJ, Cavallero E, et al. Treatment of dry age-related macular degeneration. *Ophthalmic Res*. 2014;52:107–115.

6. Curcio CA, Messinger JD, Sloan KR, McGwin G, Medeiros NE, Spaide RF. Subretinal drusenoid deposits in non-neovascular age-related macular degeneration: morphology, prevalence, topography, and biogenesis model. *Retina*. 2013;33:265–276.

7. Mullins RF, Johnson MN, Faidley EA, Skeie JM, Huang J. Choriocapillaris vascular dropout related to density of drusen in human eyes with early age-related macular degeneration. *Invest Ophthalmol Vis Sci*. 2011;52:1606–1612.

8. Ramrattan RS, van der Schaft TL, Mooy CM, de Bruijn WC, Mulder PG, de Jong PT. Morphometric analysis of Bruch's membrane, the choriocapillaris, and the choroid in aging. *Invest Ophthalmol Vis Sci*. 1994;35:2857–2864.

9. Esmaeelpour M, Ansari-Shahrezaei S, Glittenberg C, et al. Choroid, Haller's, and Sattler's layer thickness in intermediate age-related macular degeneration with and without fellow neovascular eyes. *Invest Ophthalmol Vis Sci*. 2014;55:5074–5080.

10. Vitale S, Clemons TE, Agrón E, et al. Evaluating the validity of the age-related eye disease study grading scale for age-related macular degeneration. *JAMA Ophthalmol*. 2016;134:1041–1047.

11. Gangnon RE, Lee KE, Klein BEK, Iyengar SK, Sivakumaran TA, Klein R. Severity of age-related macular degeneration in 1 eye and the incidence and progression of age-related macular degeneration in the fellow eye. *JAMA Ophthalmol*. 2015;133:125–132.

12. Spaide RF. Choriocapillaris flow features follow a power law distribution: implications for characterization and mechanisms of disease progression. *Am J Ophthalmol*. 2016;170:58–67.

13. Al-Sheikh M, Phasukkijwatana N, Dolz-Marco R, et al. Quantitative OCT angiography of the retinal microvasculature and the choriocapillaris in myopic eyes. *Invest Ophthalmol Vis Sci*. 2017;58:2063–2069.

14. Spaide RF, Fujimoto JG, Waheed NK. Image artifacts in optical coherence tomography angiography. *Retina*. 2015;35:2163–2180.

15. Choi W, Moult EM, Waheed NK, et al. Ultrahigh-speed, swept-source optical coherence tomography angiography in non-exudative age-related macular degeneration with geographic atrophy. *Ophthalmology*. 2015;122:2532–2544.

16. Spaide RF. Choriocapillaris signal voids in maternally inherited diabetes and deafness and in pseudoxanthoma elasticum

[published online ahead of print January 13, 2017]. *Retina*. doi:10.1097/IAE.0000000000001497.

17. Ferris FL, Wilkinson CP, Bird A, et al. Clinical classification of age-related macular degeneration. *Ophthalmology*. 2013;120:844–851.

18. Iafe NA, Phasukkijwatana N, Chen X, Sarraf D. Retinal capillary density and foveal avascular zone area are age-dependent: quantitative analysis using optical coherence tomography angiography. *Invest Ophthalmol Vis Sci*. 2016;57:5780–5787.

19. Jia Y, Tan O, Tokayer J, et al. Split-spectrum amplitude-decorrelation angiography with optical coherence tomography. *Opt Express*. 2012;20:4710–4725.

20. Kraus MF, Potsaid B, Mayer MA, et al. Motion correction in optical coherence tomography volumes on a per A-scan basis using orthogonal scan patterns. *Biomed Opt Express*. 2012;3:1182–1199.

21. Kraus MF, Liu JJ, Schottenhamml J, et al. Quantitative 3D-OCT motion correction with tilt and illumination correction, robust similarity measure and regularization. *Biomed Opt Express*. 2014;5:2591–613.

22. Kim AY, Chu Z, Shahidzadeh A, Wang RK, Puliafito CA, Kashani AH. Quantifying microvascular density and morphology in diabetic retinopathy using spectral-domain optical coherence tomography angiography. *Invest Ophthalmol Vis Sci*. 2016;57:OCT362–OCT370.

23. Nesper PL, Soetikno BT, Fawzi AA. Choriocapillaris non-perfusion is associated with poor visual acuity in eyes with reticular pseudodrusen. *Am J Ophthalmol*. 2017;174:42–55.

24. Schneider CA, Rasband WS, Eliceiri KW. NIH Image to ImageJ: 25 years of image analysis. *Nat Methods*. 2012;9:671–675.

25. Lane M, Moult EM, Novais EA, et al. Visualizing the choriocapillaris under drusen: comparing 1050-nm swept-source versus 840-nm spectral-domain optical coherence tomography angiography. *Invest Ophthalmol Vis Sci*. 2016;57:OCT585–OCT590.

26. Holladay JT. Proper method for calculating average visual acuity. *J Refract Surg*. 1997;13:388–391.

27. Seddon JM, McLeod DS, Bhutto IA, et al. Histopathological insights into choroidal vascular loss in clinically documented cases of age-related macular degeneration. *JAMA Ophthalmol*. 2016;134:1272–1280.

28. Saint-Geniez M, Kurihara T, Sekiyama E, Maldonado AE, D'Amore PA. An essential role for RPE-derived soluble VEGF in the maintenance of the choriocapillaris. *Proc Natl Acad Sci U S A*. 2009;106:18751–18756.

29. Cabrera AP, Bhaskaran A, Xu J, et al. Senescence increases choroidal endothelial stiffness and susceptibility to complement injury: implications for choriocapillaris loss in AMD. *Invest Ophthalmol Vis Sci*. 2016;57:5910–5918.

30. Moore DJ, Hussain AA, Marshall J. Age-related variation in the hydraulic conductivity of Bruch's membrane. *Invest Ophthalmol Vis Sci*. 1995;36:1290–1297.

31. Pilgrim MG, Lengyel I, Lanzirotti A, et al. Subretinal pigment epithelial deposition of drusen components including hydroxyapatite in a primary cell culture model. *Invest Ophthalmol Vis Sci*. 2017;58:708–719.

32. McLeod DS, Grebe R, Bhutto I, Merges C, Baba T, Lutty GA. Relationship between RPE and choriocapillaris in age-related macular degeneration. *Invest Ophthalmol Vis Sci*. 2009;50:4982–4991.

33. Kuehlewein L, Sadda SR, Sarraf D. OCT angiography and sequential quantitative analysis of type 2 neovascularization after ranibizumab therapy. *Eye*. 2015;29:932–935.

34. Kuehlewein L, Bansal M, Lenis TL, et al. Optical coherence tomography angiography of type 1 neovascularization in age-related macular degeneration. *Am J Ophthalmol*. 2015;160:739–748.e2.

35. Moult E, Choi W, Waheed NK, et al. Ultrahigh-speed swept-source OCT angiography in exudative AMD. *Ophthalmic Surg Lasers Imaging Retina*. 2014;45:496–505.

36. Toto L, Borrelli E, Mastropasqua R, et al. Association between outer retinal alterations and microvascular changes in intermediate stage age-related macular degeneration: an optical coherence tomography angiography study [published online ahead of print September 13, 1016]. *Br J Ophthalmol*. doi:10.1136/bjophthalmol-2016-309160.

37. Moult EM, Waheed NK, Novais EA, et al. Swept-source optical coherence tomography angiography reveals choriocapillaris alterations in eyes with nascent geographic atrophy and drusen-associated geographic atrophy. *Retina*. 2016;36:S2–S11.

38. Rogala J, Zangerl B, Assaad N, Fletcher EL, Kalloniatis M, Nivison-Smith L. In vivo quantification of retinal changes associated with drusen in age-related macular degeneration. *Invest Ophthalmol Vis Sci*. 2015;56:1689–1700.

39. Mullins RF, Johnson MN, Faidley EA, Skeie JM, Huang J. Choriocapillaris vascular dropout related to density of drusen in human eyes with early age-related macular degeneration. *Invest Ophthalmol Vis Sci*. 2011;52:1606–1612.

40. Mendrinos E, Mangioris G, Papadopoulou DN, Donati G, Pournaras CJ. Long-term results of the effect of intravitreal ranibizumab on the retinal arteriolar diameter in patients with neovascular age-related macular degeneration. *Acta Ophthalmol*. 2013;91:e184–e190.

41. Hanhart J, Tiosano L, Averbukh E, et al. Fellow eye effect of unilateral intravitreal bevacizumab injection in eyes with diabetic macular edema. *Eye*. 2014;28:646–653.

42. Velez-Montoya R, Fromow-Guerra J, Burgos O, Landers MB, Morales-Catón V, Quiroz-Mercado H. The effect of unilateral intravitreal bevacizumab (avastin), in the treatment of diffuse bilateral diabetic macular edema: a pilot study. *Retina*. 2009;29:20–26.

43. Wu Z, Sadda SR. Effects on the contralateral eye after intravitreal bevacizumab and ranibizumab injections: a case report. *Ann Acad Med Singapore*. 2008;37:591–593.